Science Translational Medicine
AAAS

stm.sciencemag.org/cgi/content/full/13/593/eabf6356/DC1

# Supplementary Materials for

## A portable magnetofluidic platform for detecting sexually transmitted infections and antimicrobial susceptibility

Alexander Y. Trick, Johan H. Melendez, Fan-En Chen, Liben Chen, Annet Onzia, Aidah Zawedde, Edith Nakku-Joloba, Peter Kyambadde, Emmanuel Mande, Joshua Matovu, Maxine Atuheirwe, Richard Kwizera, Elizabeth A. Gilliams, Yu-Hsiang Hsieh, Charlotte A. Gaydos, Yukari C. Manabe, Matthew M. Hamill, Tza-Huei Wang*

*Corresponding author. Email: thwang@jhu.edu

Published 12 May 2021, *Sci. Transl. Med.* **13**, eabf6356 (2021)
DOI: 10.1126/scitranslmed.abf6356

**The PDF file includes:**

Materials and Methods
Fig. S1. PROMPT instrument housing.
Fig. S2. *N. gonorrhoeae* lysis evaluation.
Fig. S3. Finite-element heat transfer simulations for aluminum well design.
Fig. S4. Finite-element heat transfer simulations for aluminum heat block dimensions.
Fig. S5. Heat block thermocycling characterization.
Fig. S6. Cartridge fabrication.
Fig. S7. Cartridge shelf-life.
Fig. S8. Linear regression algorithm for $C_t$ determination.
Fig. S9. $C_t$ determination visualization.
Fig. S10. Kampala clinical testing workflow.
Fig. S11. End-user survey responses.
Fig. S12. End-user survey respondent data.
Fig. S13. Binding buffer adjustment.
Fig. S14. Magnetic bead interactions with PCR reagents.
Table S1. Cartridge assay validation with *N. gonorrhoeae* isolates.
Table S2. Cartridge assay specificity evaluation.
Table S3. Archived Baltimore clinical sample validation.
Table S4. Discrepant PROMPT results in clinical validation.
Table S5. Duplexed PCR assay buffer.
Table S6. PCR primers and probes.

**Other Supplementary Material for this manuscript includes the following:**

(available at stm.sciencemag.org/cgi/content/full/13/593/eabf6356/DC1)

Data file S1 (Microsoft Excel format). Shelf-life data.
Data file S2 (Microsoft Excel format). *N. gonorrhoeae* PROMPT cartridge data.
Data file S3 (.pdf format). Survey questions.
Movie S1 (.mp4 format). PROMPT platform operation.

## Supplementary Materials:

### Materials and Methods

*Rapid PCR assay optimization and verification*

To assess the optimal primer and enzyme (SpeedSTAR HS, Takara Bio) conditions for rapid PCR, all combinations of *opa* primer concentrations 0.3, 0.6 , 1, 2, or 3 µM and enzyme concentrations (0.25, 0.5, 1, 2.5 Units/reaction) were tested with target input of $10^6$ CFU ATCC 49226 in a final reaction volume of 10 µL. In addition to the primers and enzyme, each PCR reaction consisted of final concentrations of 1X SpeedSTAR Fast I buffer, 200 µM dNTPs, 1X Evagreen, and 0.2% v/v Tween-20. Real-time PCR was implemented on a benchtop thermocycler (BioRad CFX96) with a 30 sec 95°C hot-start incubation followed by 40 cycles of denaturation for 1 sec at 95°C and annealing at 62°C for 1 sec. Thermocycling was immediately followed by melt-curve analysis on the same instrument by ramping from 60°C to 95°C with fluorescence detection at 0.5°C increments. Ct values were calculated using the BioRad CFX manager regression determination mode.

*Finite-element heat transfer simulations*

Aluminum heat blocks were simulated using the heat transfer and CFD modules in COMSOL Multiphysics Software v5.1. For evaluating the effects of well aspect ratio and heat block volume on PCR temperature ramp rates, a parametric sweep of well aspect ratio (height/width) and heat block thickness was conducted with a constant power supplied to the base of the heat block (1W, 3W, or 5W) (Fig. S3). For all aspect ratios, the PCR volume was maintained at 10µL with initial temperatures of all components set at 50°C. The simulations were run until the PCR volume reached and average temperature of 100°C and the average ramp rates were calculated for 60-100°C. Similarly to assess the effect of varying thickness of the cantilevered heat block design and cross-sectional on the ramp rate, another set of parametric sweeps was conducted varying the heat block thickness, width of the "neck" region between the thermoelectric and the PCR well, and the heat power supplied to the thermoelectric region (Fig. S4).

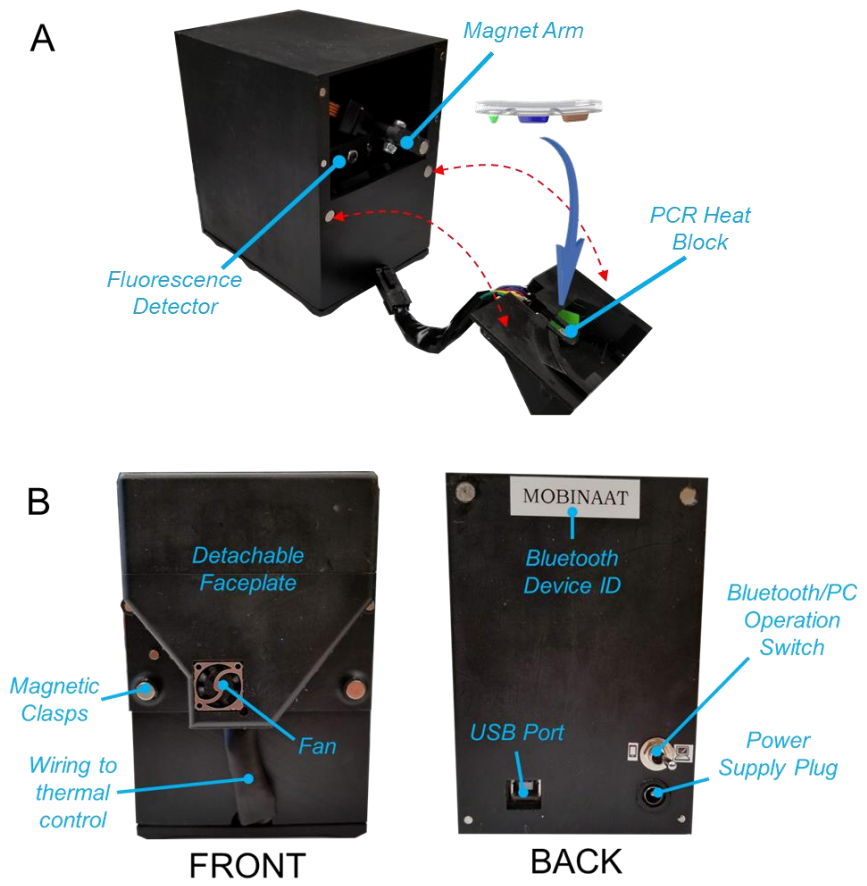


**Fig. S1. PROMPT instrument housing. (A)** The detachable faceplate allows for insertion of the magnetofluidic cartridge into the instrument with alignment back onto the housing for magnet processing and fluorescence detection for real-time PCR. **(B)** Neodymium permanent magnets hold the 3D-printed housing together and allow for faceplate attachment. Wiring from the faceplate leads to the built-in microcontroller for temperature sensing and control, and fan control to cool the TE during thermal cycling. Ports in the back of the instrument provide connections for USB to connect to a computer for running tests or programming the instrument and a power supply barrel plug for battery or AC/DC adapter. The switch in the back selects for instrument operation in either the computer (PC) or Bluetooth (smartphone) mode. When in Bluetooth mode, the user connects to the device by finding the device ID indicated on the back of the instrument.

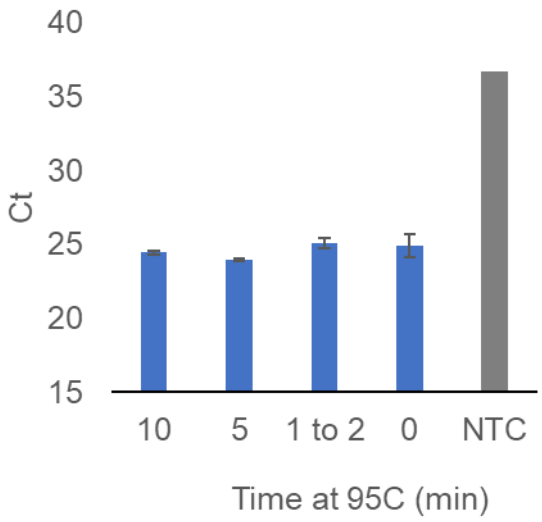


**Fig. S2. *N. gonorrhoeae* lysis evaluation.** Assessment of thermal lysis using $10^7$ CFU (ATCC 49226) followed by magnetic bead purification showed no improvement compared to no thermal lysis at all (0 min), indicating the exposure to binding buffer alone without heat treatment was sufficient to induce cell lysis. All lysis methods were followed by magnetic bead purification on benchtop using 50 µL ChargeSwitch wash buffer and elution into 10 µL ChargeSwitch elution buffer. The elution buffer was then spiked into single-plex *opa* PCR reactions in triplicate.

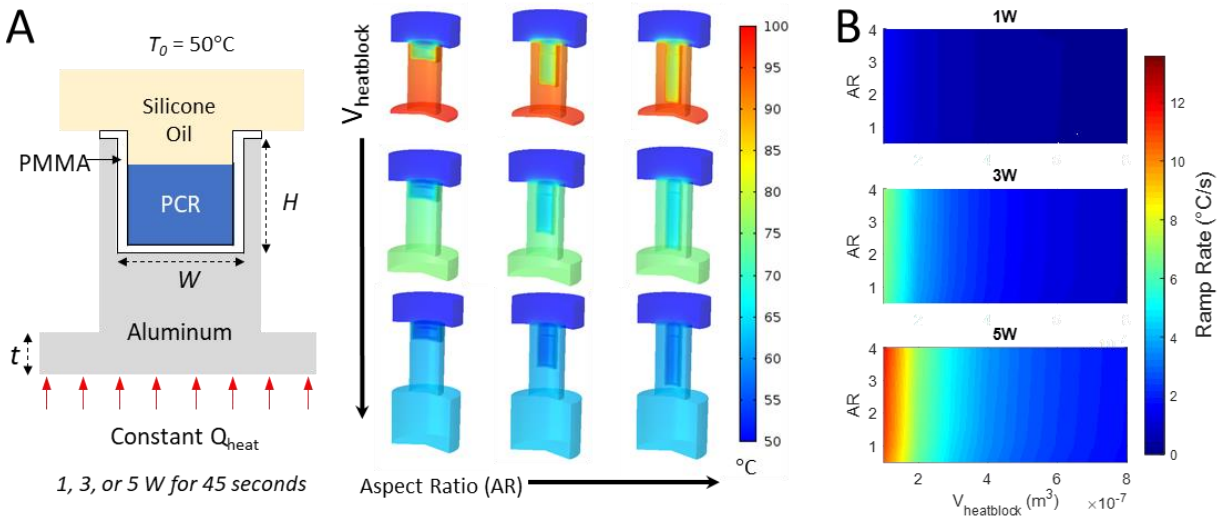


**Fig. S3. Finite-element heat transfer simulations for aluminum well design.** (A) Parametric design sweep for simulations with color-coded temperature after 45 sec of heat applied to bottom of the aluminum heat block (B) Well aspect ratio (AR) has minimal effect on the heating ramp rate of the PCR solution compared to heat block volume ($V_{heatblock}$). Aspect ratios of the well given a constant 10 µL reaction volume showed minor effects in the temperature ramp rate with a maximum CV of 6.5% for aspect ratios ranging from 0.5 to 4. This permits flexibility in well geometry for ease in ensuring compatibility with thermoforming and CNC milling manufacture of cartridges and heat blocks without sacrificing thermal performance.

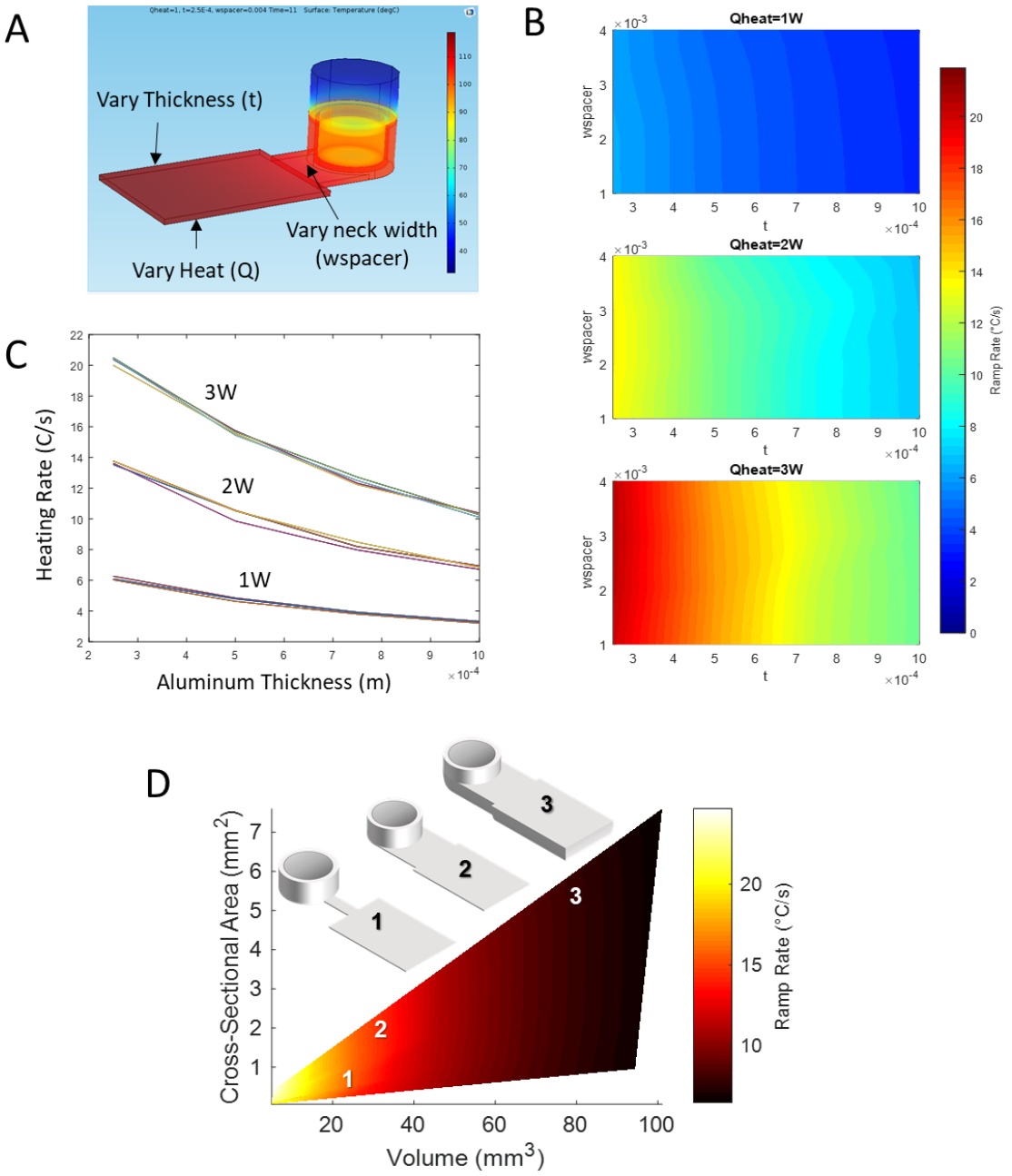


**Fig. S4. Finite-element heat transfer simulations for aluminum heat block dimensions. (A)** Parametric model of cantilevered heat block used to determine optimal dimensions for maximizing heat transfer and minimizing thermal mass. Heat is applied as at a constant power to the rectangular section designed to fit to the TE dimensions (8.2 mm x 6 mm). **(B)** Temperature ramp rates for the water volume in the heat block well given 1W, 2W, and 3W constant heat applied. **(C)** Temperature ramp rates for different heat power and heat block thickness. Each line represents a different value for the neck width (wspacer) resulting in varying cross-sectional area from the rectangular section in contact with the TE to the PCR well. (**D**) Effect of cross-sectional area vs. heat block volume on ramp rate for 3W of heat.

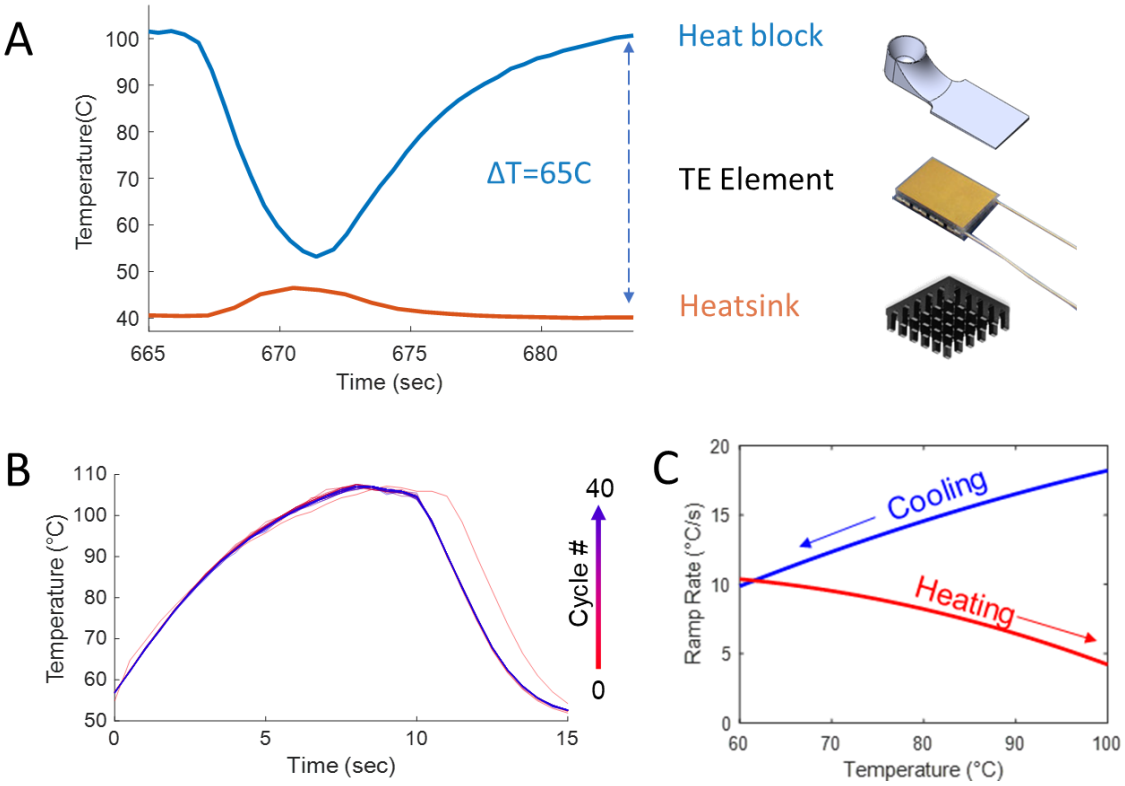


**Fig. S5. Heat block thermocycling characterization. (A)** Temperature of the heat block (blue) and heatsink (orange) during on cycle of PCR thermocycling. (**B**) Temperature profile of all 40 cycles from a single PCR assay overlaid. The first cycle (red) requires additional heating time to raise the heatsink temperature in order for the heat block to reach the target denaturation temperature. (**C**) Calculated temperature ramp rates at a given heat block temperature for heating and cooling during thermocycling.

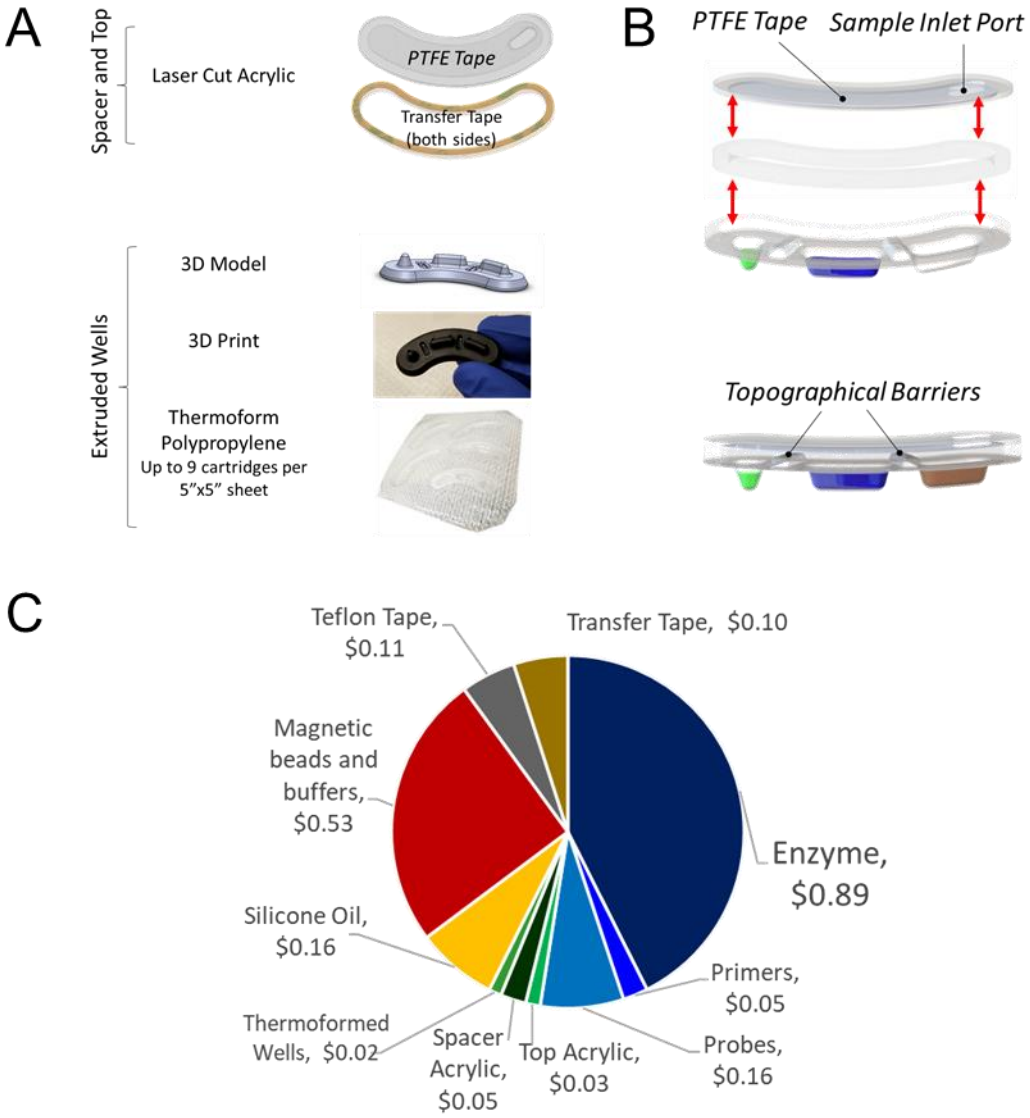


**Fig. S6. Cartridge fabrication. (A)** Each cartridge is composed of 3 layers – a laser-cut acrylic top, a laser-cut acrylic spacer laminated with transfer tape, and polypropylene wells created by thermoforming onto 3D-printed molds. (**B**) The top section has a laser-cut hole to serve as an inlet port to inject the sample and is laminated with PTFE (Teflon) tape to provide a smooth hydrophobic surface for magnetic bead transfer without sample loss. The spacer and wells are laminated with transfer tape followed by loading the PCR and wash reagents. Then using transfer tape on the opposite side of the spacer, the cartridge is sealed with the top layer. Silicone oil fills the remaining space within the cartridge to provide an immiscible barrier to escape of the aqueous reagents by evaporation or slipping out of the wells. **(C)** Over 2/3 of the raw material cost of each cartridge is attributed to the PCR reagents (enzyme, primers, probes) and the magnetic beads and buffers which would be significantly reduced when manufactured at scale. Total cost of goods including manufacturing would be minimal given the simple three-layer lamination process that avoids expensive machines and molds associated with injection molding and microfabrication techniques currently used for microfluidics and POC diagnostics products.

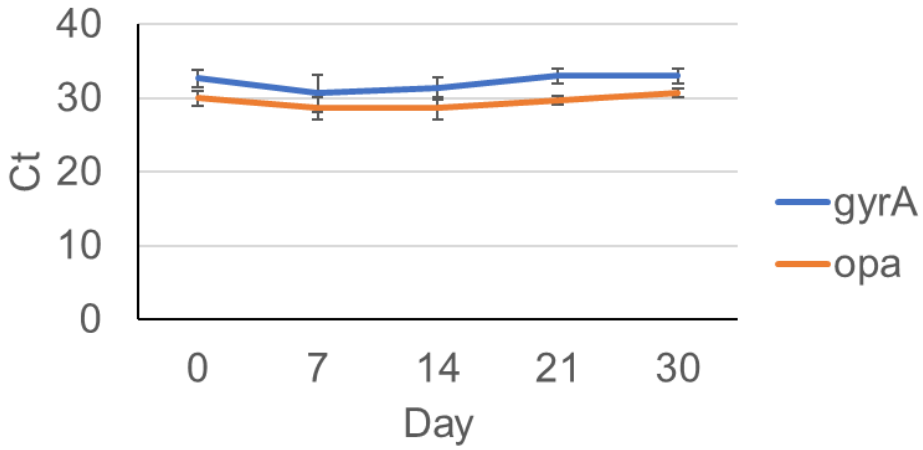


**Fig. S7. Cartridge shelf-life.** Assay cartridges were stored at -20°C and sampled at 7 day intervals for 1 month. Tests were run in triplicate on day 0 prior to freezing cartridges and each following week using $10^6$ CFU ATCC 49226 sample input.

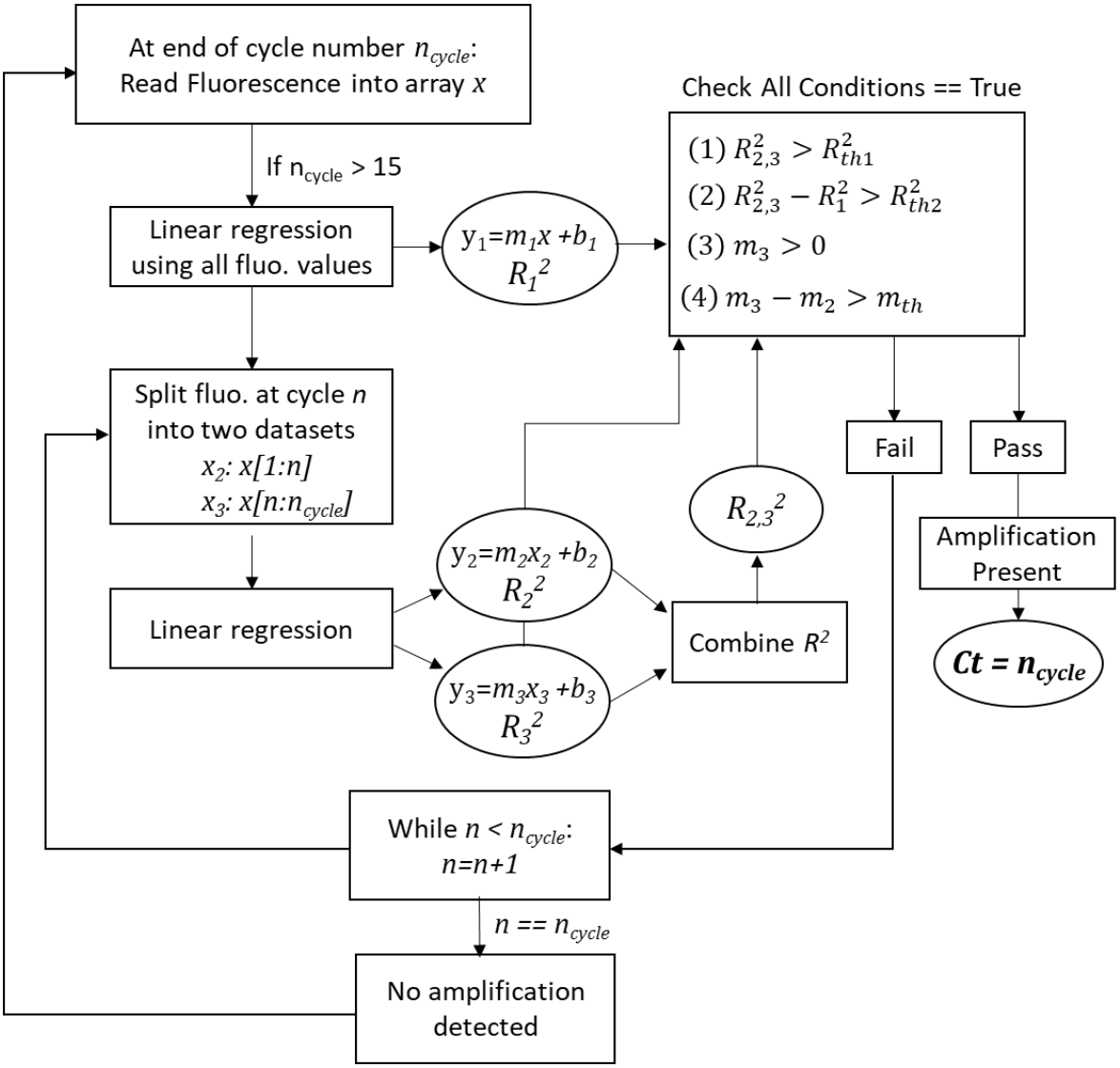


**Fig. S8. Linear regression algorithm for $C_t$ determination.**

After cycle 15 of PCR, each subsequent fluorescence acquisition from following cycles triggers the GUI software to process the data using a custom linear regression algorithm to determine the amplification status of each target. For each fluorescent channel, the real-time fluorescence is fit to a linear regression curve ($y_1$) and the coefficient of determination is calculated ($R_1^2$). Then the data is split at cycle $n$, where $n$ is an integer cycle number starting at cycle 12 where the resulting two sets of fluorescence data for cycles 1 through $n$ or $n$ through the last cycle, $n_{cycle}$, are separately are fit with linear regression to generate linear equations $y_2$ and $y_3$ with $R_2^2$ and $R_3^2$ for the respective first and second sets. Each $R^2$ value is calculated as follows:

$$R^2 = 1 - \left(\frac{SS_{res}}{SS_{tot}}\right) \qquad (1.1)$$

where given the raw fluorescence data, $y$, at each cycle $i$, and the regression fit value, $f$, the regression sum of squares, $SS_{res}$, and total sum of squares, $SS_{tot}$, are defined as

$$SS_{res} = \sum_i (y_i - \bar{y})^2 \qquad (1.2)$$

$$SS_{tot} = \sum_i (f_i - \bar{y})^2 \qquad (1.3)$$

The combined $R^2$ value from both $R_2^2$ and $R_3^2$ is then calculated with the following relationship:

$$R_{2,3}^2 = 1 - \left(\frac{SS_{res,2} + SS_{res,3}}{SS_{tot,2} + SS_{tot,3}}\right) \qquad (1.4)$$

For the given split cycle, *n*, the following conditions are checked:

$$R_{2,3}^2 > R_{th1}^2 \qquad (2.1)$$

$$R_{2,3}^2 - R_1^2 > R_{th2}^2 \qquad (2.2)$$

$$m_3 > 0 \qquad (2.3)$$

$$m_3 - m_2 > m_{th} \qquad (2.4)$$

where *m* is the slope of a given fit and $R_{th1}^2$, $R_{th2}^2$, and $m_{th}$ are experimentally determined threshold constants. If one of these conditions are not met, the process is repeated for a split at cycle $n + 1$. If all conditions pass, then amplification is present and the Ct is reported in real-time at the current PCR cycle. For the *opa* and *gyrA* assays, the threshold constants are defined as $R_{th1}^2 = 0.5$, $R_{th2}^2 = 0.2$, and $m_{th} = 3$.

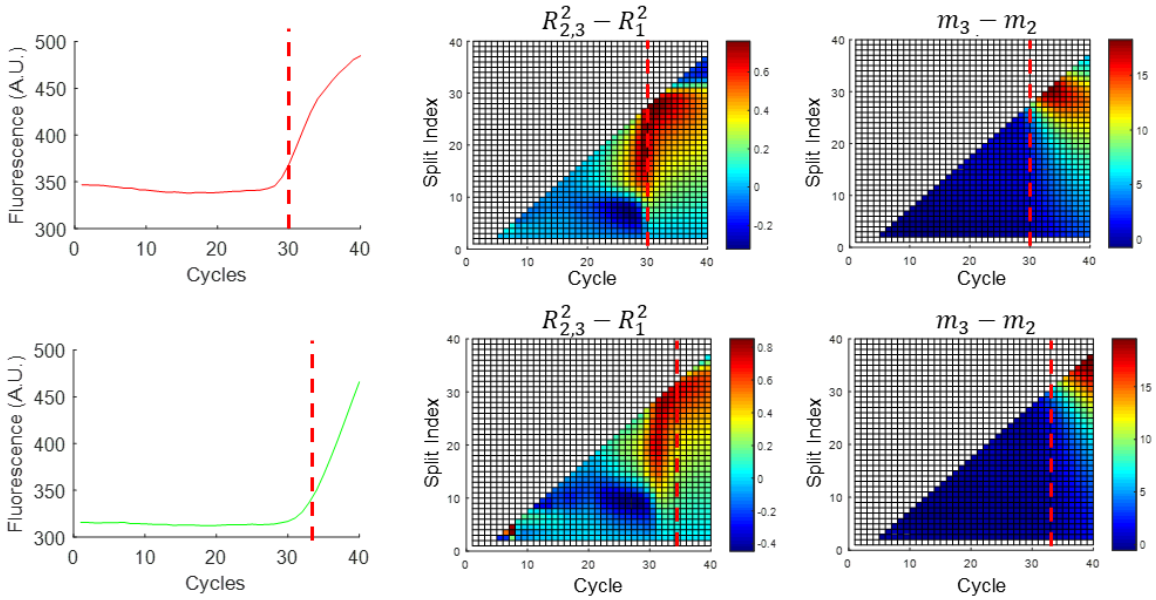


**Fig. S9. $C_t$ determination visualization.** Ct algorithm detection of amplification for *opa* (top) and *gyrA* (bottom) fluorescence signals. Results for checking conditions in eqns. 2.2 and 2.4 are plotted for all cycle splits with Ct reported at cycle 30 and 33 for *opa* and *gyrA* respectively indicated by the red dashed line.

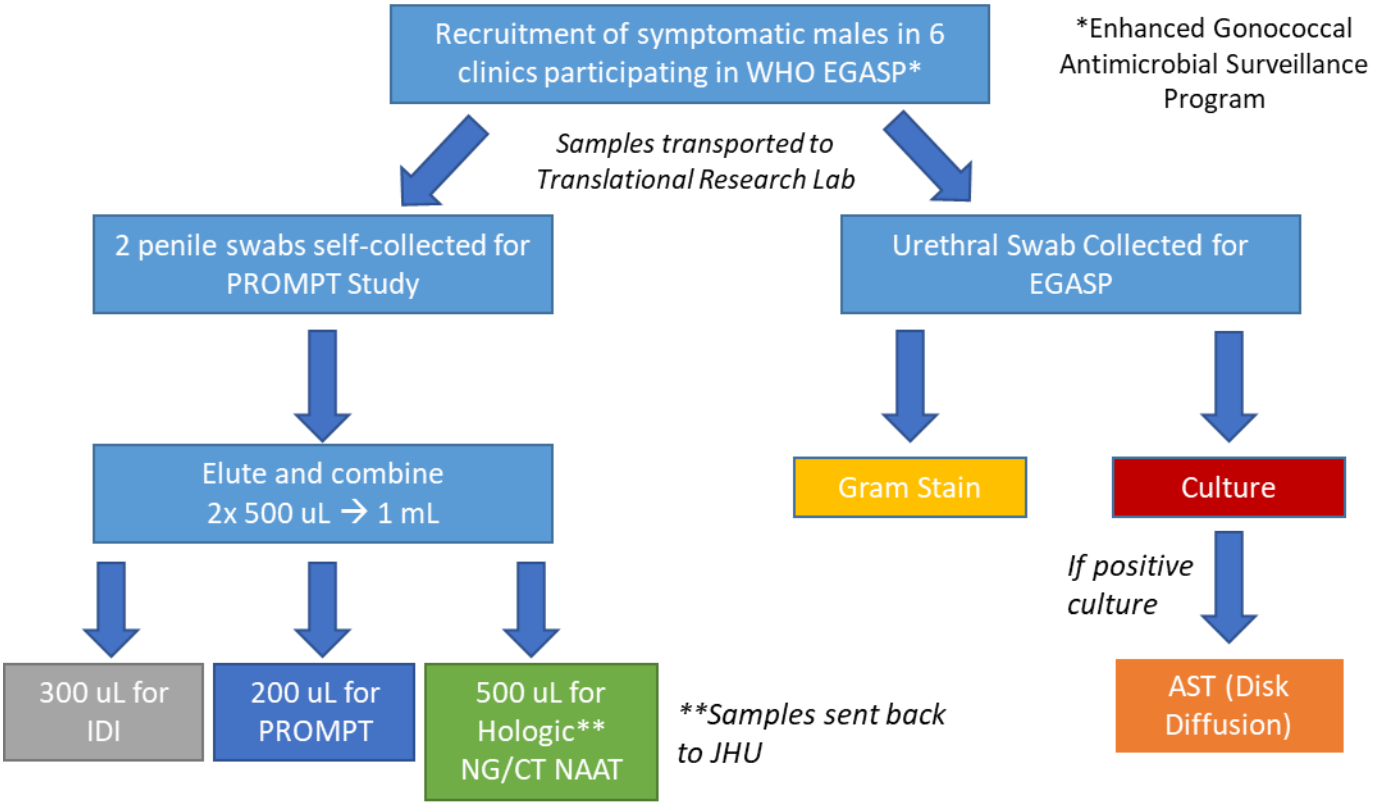


**Fig. S10. Kampala clinical testing workflow.**

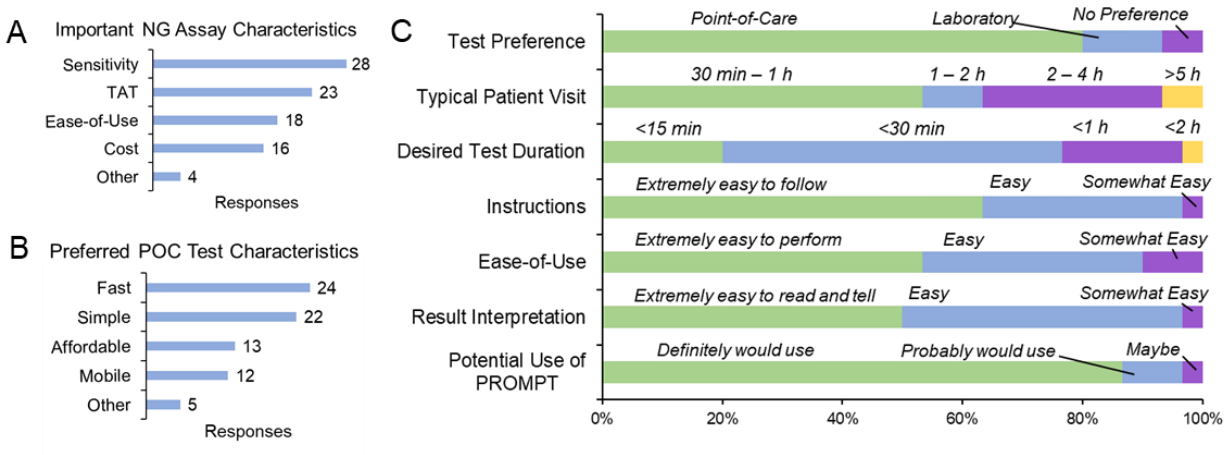


**Fig. S11. End-user survey responses.** Survey responses from 30 clinicians and laboratory technicians in Kampala, Uganda involved in diagnosis and treatment of STIs (**A**) The most important characteristics selected for a *N. gonorrhoeae* diagnostic. (**B**) Desired characteristics for a POC *N. gonorrhoeae* test. (**C**) Responder feedback after viewing a demonstration of the PROMPT platform in use (movie S1).

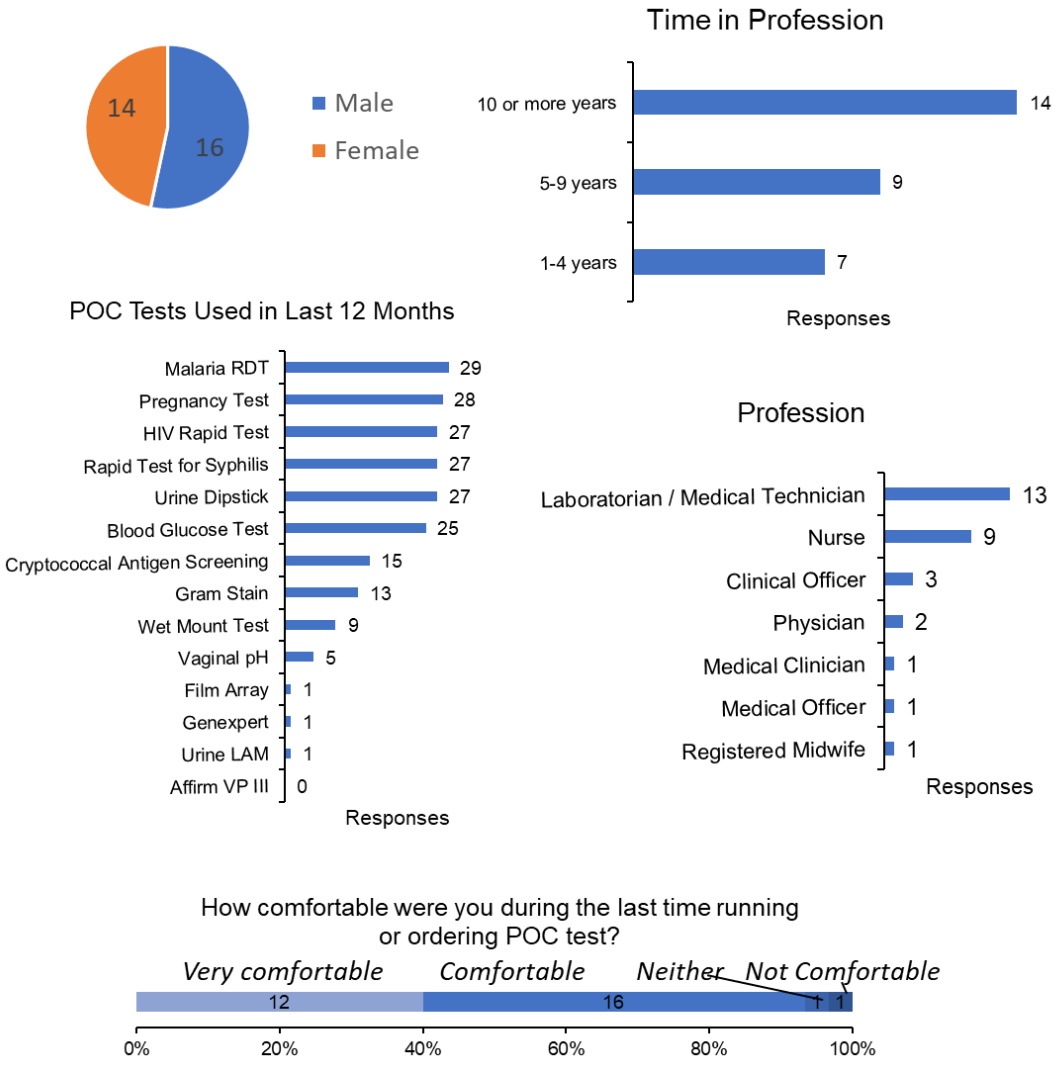


**Fig. S12. End-user survey respondent data.**

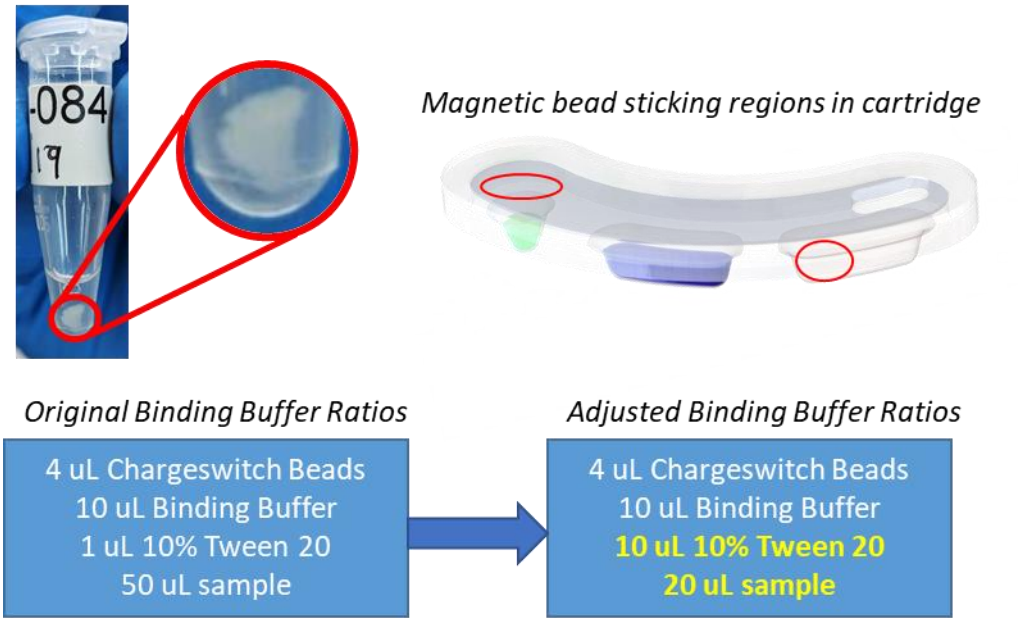


**Fig. S13. Binding buffer adjustment.** Due to large amounts of aggregated cellular debris (top-left) encountered in several of the Kampala swab eluates compared to the BCHD samples previously processed, bead transfer was occasionally inhibited with sticking of the beads to the internal plastic of the cartridge. To address this for the Kampala samples, the binding buffer with magnetic beads used in sample processing was adjusted to include more surfactant (Tween-20) for solubilizing protein matter and a reduced volume of samples was introduced into the cartridge.

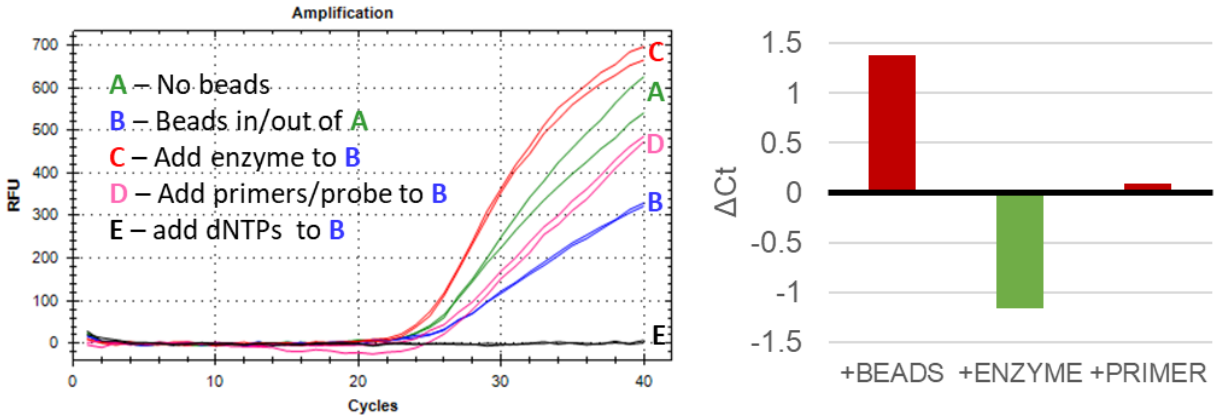


**Fig. S14. Magnetic bead interactions with PCR reagents.** To assess the effect of introducing magnetic beads into the PCR assay, 10 µL volumes of PCR with $10^6$ CFU NG cells were (A) run directly with benchtop PCR, or (B) exposed to 100µg washed magnetic beads. After exposure to beads, the original assay amounts of enzyme (0.25 Units – C), primers/probe (0.3 µM/0.25µM – D), or dNTPs (200 µM - E) were added back into the PCR mixes. All conditions were run in duplicate. Introduction of the beads increased the Ct value by ~1.4 cycles while adding back enzyme recovered and improved amplification with a Ct reduction of ~1.2 cycles. Addition of primers and probe after bead exposure recovered amplification to the approximately the original direct spike Ct (ΔCt ~ 0.1).

**Table S1. Cartridge assay validation with *N. gonorrhoeae* isolates.**

| # | Source | Sample ID | PROMPT Ct - *opa* | PROMPT Ct - *gyrA* | Ciprofloxacin MIC | Agreement |
|---|---|---|---|---|---|---|
| 1 | BCHD | 0101 | 23 | #N/A | 4 | Yes |
| 2 | BCHD | 0102 | 21 | #N/A | 32 | Yes |
| 3 | BCHD | 0119 | 24 | #N/A | 2 | Yes |
| 4 | BCHD | 0315 | 19 | #N/A | 4 | Yes |
| 5 | BCHD | 0316 | 25 | #N/A | 0.125 | Yes |
| 6 | BCHD | 0407 | 21 | #N/A | 12 | Yes |
| 7 | BCHD | 0411 | 20 | #N/A | 2 | Yes |
| 8 | BCHD | 0610 | 20 | #N/A | 2 | Yes |
| 9 | BCHD | 0704 | 22 | #N/A | 32 | Yes |
| 10 | BCHD | 0713 | 23 | #N/A | 8 | Yes |
| 11 | BCHD | 0810 | 25 | #N/A | 2 | Yes |
| 12 | BCHD | 0912 | 20 | #N/A | 4 | Yes |
| 13 | BCHD | 0926 | 28 | #N/A | 32 | Yes |
| 14 | BCHD | 1006 | 21 | #N/A | 4 | Yes |
| 15 | BCHD | 1011 | 32 | #N/A | 8 | Yes |
| 16 | BCHD | 0107 | 20 | 23 | 0.002 | Yes |
| 17 | BCHD | 0115 | 20 | 21 | 0.003 | Yes |
| 18 | BCHD | 0301 | 21 | 22 | 0.002 | Yes |
| 19 | BCHD | 0309 | 24 | 28 | 0.002 | Yes |
| 20 | BCHD | 0310 | 26 | 29 | 0.002 | Yes |
| 21 | BCHD | 0401 | 22 | 24 | 0.002 | Yes |
| 22 | BCHD | 0403 | 26 | 28 | 0.003 | Yes |
| 23 | BCHD | 0406 | #N/A | 23 | 0.003 | No* |
| 24 | BCHD | 0504 | 23 | 27 | 0.003 | Yes |
| 25 | BCHD | 0505 | 25 | 26 | 0.002 | Yes |
| 26 | BCHD | 0509 | 22 | 24 | 0.003 | Yes |
| 27 | BCHD | 0604 | 19 | 21 | 0.003 | Yes |
| 28 | BCHD | 0608 | 23 | 26 | 0.003 | Yes |
| 29 | BCHD | 0611 | 22 | 24 | 0.002 | Yes |
| 30 | BCHD | 0613 | 25 | 27 | 0.002 | Yes |
| 31 | BCHD | 0911 | 26 | 26 | 0.003 | Yes |
| 32 | BCHD | 0916 | 28 | 29 | 0.003 | Yes |
| 33 | BCHD | 0928 | 21 | 27 | 0.002 | Yes |
| 34 | BCHD | 1015 | 29 | 29 | 0.002 | Yes |
| 35 | BCHD | 1016 | 20 | 22 | 0.003 | Yes |
| 36 | ATCC | 49226 | 23 | 30 | 0.004 | Yes |
| 37 | WHO | WHO K | 22 | #N/A | >32 | Yes |
| 38 | WHO | WHO L | 21 | #N/A | >32 | Yes |

#N/A = No amplification

*Isolate 0406 from BCHD tested false-negative with the *opa* assay on cartridge. Confirmation that this isolate was indeed NG was conducted with positive amplification of in-house PCR assays for an NG *porA* sequence. Benchtop PCR with intercalating dye (Evagreen) instead of probe produced positive amplification profiles, further indicating lack of cartridge amplification was an issue of *opa* probe sequence mismatch.

**Table S2. Cartridge assay specificity evaluation.**

| Sample | Ct- *gyrA* | Ct- *opa* |
|---|---|---|
| *N. perflava* | #N/A | #N/A |
| *N. mucosa* | 30 | #N/A |
| *N. lactamica* | #N/A | #N/A |
| *N. cinerea* | #N/A | #N/A |
| *N. sicca* | #N/A | #N/A |
| *N. meningitidis* | #N/A | #N/A |
| *S. epidermis* | #N/A | #N/A |
| *E. coli* | #N/A | #N/A |
| *Herpes Simplex Virus - type 1* | #N/A | #N/A |
| *C. trachomatis - serovar D* | #N/A | #N/A |
| *C. trachomatis - serovar E* | #N/A | #N/A |
| *C. trachomatis - serovar F* | #N/A | #N/A |
| *C. trachomatis - serovar G* | #N/A | #N/A |
| *Trichomonas vaginalis* | #N/A | #N/A |
| *Lactobacillus* | #N/A | #N/A |

#N/A = No amplification

**Table S3. Archived Baltimore clinical sample validation.**

| # | Sample ID | PROMPT Ct - *opa* | PROMPT Ct - *gyrA* | Hologic NG Results |
|---|---|---|---|---|
| 1 | 080 | #N/A | #N/A | Negative |
| 2 | 093 | #N/A | #N/A | Negative |
| 3 | 097 | #N/A | #N/A | Negative |
| 4 | 109 | #N/A | #N/A | Negative |
| 5 | 111 | #N/A | #N/A | Negative |
| 6 | 244 | #N/A | #N/A | Negative |
| 7 | 318 | #N/A | #N/A | Negative |
| 8 | 338 | #N/A | #N/A | Negative |
| 9 | 357 | #N/A | #N/A | Negative |
| 10 | 358 | #N/A | #N/A | Negative |
| 11 | 385 | #N/A | #N/A | Negative |
| 12 | 392 | #N/A | #N/A | Negative |
| 13 | 405 | #N/A | #N/A | Negative |
| 14 | 433 | #N/A | #N/A | Negative |
| 15 | 081 | 29 | 31 | Positive |
| 16 | 091 | 29 | #N/A | Positive |
| 17 | 092 | 31 | 33 | Positive |
| 18 | 096 | 36 | 37 | Positive |
| 19 | 110 | 35 | 37 | Positive |
| 20 | 236 | 33 | #N/A | Positive |
| 21 | 278 | 32 | 33 | Positive |
| 22 | 291 | 33 | #N/A | Positive |
| 23 | 350 | 35 | 38 | Positive |
| 24 | 391 | 33 | 33 | Positive |
| 25 | 404 | 27 | #N/A | Positive |
| 26 | 426 | 30 | 34 | Positive |
| 27 | 436 | 35 | 34 | Positive |
| 28 | 437 | 36 | #N/A | Positive |
| 29 | 440 | 36 | 33 | Positive |
| 30 | 462 | 29 | 30 | Positive |
| 31 | MSCS024 | 29 | 31 | Positive |
| 32 | MSCS138 | 31 | 32 | Positive |

#N/A = No amplification

## Table S4. Discrepant PROMPT results in clinical validation.

| Participant Number | PROMPT Results | PROMPT *opa* CT | Hologic NG (swab) | Hologic NG (urine) | Culture | Comments |
|---|---|---|---|---|---|---|
| *PROMPT Positive with Conflicting Hologic Results* | | | | | | |
| MN-126 | Positive | 32 | Equivocal | Positive | Positive | Hologic NG testing on swab sample produced negative results, but culture and urine testing showed NG-positive, so both samples included as NG-positive in agreement with PROMPT results |
| MN-128 | Positive | 37 | Negative | Positive | Positive | |
| *PROMPT False-Negative vs. Hologic Results* | | | | | | |
| MN-011 | Negative | 40 | Positive | N/A | Positive | Cartridges failed to detect positive samples. |
| MN-098 | Negative | 40 | Positive | Positive | Positive | |
| MN-185 | Negative | 40 | Positive | N/A | Negative | |
| *PROMPT False-Positive vs. Hologic Results* | | | | | | |
| MN-005 | Late Ct | 38 | Negative | Negative | Negative | Late Ct on PROMPT due to cartridge contamination or nonspecific amplification allows exclusion by Ct thresholding (Ct >37). |
| MN-059 | Late Ct | 38 | Negative | Negative | Negative | |
| MN-076 | Late Ct | 38 | Negative | Negative | Negative | |
| MN-077 | Positive | 35 | Negative | Negative | Negative | PROMPT positive likely due to cartridge contamination by user. |
| *PROMPT Positive with Conflicting Hologic vs. Culture Results* | | | | | | |
| MN-064 | Positive | 36 | Negative | Negative | Positive | Positive cartridges match Uganda culture results, but NG undetected by Hologic NAAT. These samples were confirmed as true positives by in-house benchtop PCR and included as NG-positive in agreement with PROMPT results. |
| MN-137 | Positive | 32 | Negative | Negative | Positive | |

**Table S5. Duplexed PCR assay buffer.**

| Component | Stock Concentration | Volume per reaction (µL) | Final concentration |
|---|---|---|---|
| 10X SpeedSTAR FAST I buffer | 10X | 1 | 1X |
| Forward Primer -opa | 100 µM | 0.2 | 2 µM |
| Reverse Primer - opa | 100 µM | 0.2 | 2 µM |
| Forward Primer - gyrA | 100 µM | 0.2 | 2 µM |
| Reverse Primer - gyrA | 100 µM | 0.2 | 2 µM |
| dNTP mix | 10000 µM | 0.2 | 200 µM |
| Probe - opa (Cy5) | 10 µM | 1 | 1 µM |
| Probe - gyrA (FAM) | 10 µM | 1 | 1 µM |
| SpeedSTAR DNA Polymerase | 5 U/µL | 0.2 | 0.1 U/µL |
| 10% v/v Tween 20 | 10% | 0.2 | 0.2% |
| dH2O | n/a | 5.6 | n/a |

**Table S6. PCR primers and probes.**

| Sequence Target | Primer/Probe/Target | Sequence | Source |
|---|---|---|---|
| opa | Forward Primer | TTG AAA CAC CGC CCG GAA | Tabrizi 2005 (*24*) |
| | Reverse Primer | TTT CGG CTC CTT ATT CGG TTT AA | |
| | Probe | /5Cy5/CCG ATA TAA /TAO/TCC GTC CTT CAA CAT CAG /3IAbRQSp/ | |
| gyrA | Forward Primer | TTG CGC CAT ACG GAC GAT | Giles 2004 (*25*) |
| | Reverse Primer | GCG ACG TCA TCG GTA AAT ACC A | |
| | Probe | /56-FAM/TGT CGT AAA /ZEN/CTG CGG AA/3IABkFQ/ | |